Detailed reconstruction for coronary arteries integrating angiographies and IVUS studies

G. D. Maso Talou [1,2], P. J. Blanco[1,2], I. Larrabide[3], C. Guedes Bezerra[4], P. A. Lemos[4], and R. A. Feijóo[1,2]

[1]National Laboratory for Scientific Computing – Petrópolis, RJ – Brazil

[2]National Institute of Science and Technology
in Medicine Assisted by Scientific Computing (INCT/MACC) – Brazil.

[3]National Scientific and Technical Research Council
Pladema – CONICET – Tandil, BA – Argentina

[4]Department of Interventional Cardiology – Heart Institute (InCor)
University of São Paulo Medical School – São Paulo, SP – Brazil

{gonzalot,pjblanco,feij}@lncc.br,

ignacio.larrabide@gmail.com,

{Pedro.lemos, cristiano.bezerra}@incor.usp.br

Abstract. *The early prediction and/or detection of cardiovascular diseases are of paramount importance worldwide due to the increasing mortality and morbidity rate in the global population. Specifically, key factors for its assessment such as atherosclerotic plaque evolution and vulnerability in coronary arteries are still poorly understood, although in the last decade emerging techniques based on computational models provided a complementary approach towards these problems. To apply these models to patient specific scenarios, a geometric representation of the patient coronary vessels must be accurately constructed in three dimensional space. To achieve this purpose, we present a reconstruction methodology that aims to integrate the high definition provided by intravascular ultrasound about the vessel structure, with the spatial information presented in orthogonal angiographies. As result, the three-dimensional geometric reconstruction of the vessel at different cardiac phases along the cardiac cycle can be obtained, enabling the subsequent development of patient-specific computational models.*

1. Introduction

Cardiovascular diseases are the leading cause of death and morbidity worldwide. The detection and quantification of atherosclerosis is of the highest importance to monitor treatment and prevention of acute events. For this reason, accurate and robust techniques to assess and visualize the atherosclerotic plaque are key for an effective treatment of the disease. Remarkably, the genesis, evolution and rupture conditions of the plaque are not completely understood [Naghavi et al. 2003, Caro 2009], and emerging methodologies and technologies based on physical models provide complementary tools to assist cardiovascular research.

Computational models for characterizing blood flow and fluid-structure interaction have shown progress in the identification of the key factors that play a major role in the initiation, localization, growth, composition, remodelling, and destabilization of atheromatous plaque [Wentzel et al. 2001, Feldman et al. 2002, Carlier et al. 2003, Stone et al. 2003, Wentzel et al. 2003, Chatzizisis et al. 2008, Honda and Fitzgerald 2008]. Also, these models are fully adaptable to simulate different scenarios for patients specific conditions, enabling computational experiments to quantify physical variables in locations and at scales that cannot be extracted from in-vivo studies or they suppose a very invasive and difficult task.

However, computational models require the definition of a detailed geometry of the vessel of interest in a certain patient. For this particular task, intravascular ultrasound (IVUS) provides an accurate characterization of the plaque ($\approx$ 40 μm) at the cross-sectional planes of the vessel. Nevertheless, these data is acquired in a local coordinate system attached over the catheter deployed in the vessel interior. To obtain a correct 3D reconstruction of the vessel, a mapping of this information must be performed by using a complementary study able to visualize the catheter distribution in space.

In this work we propose a reconstruction methodology that aims to integrate the high definition about the vessel internal structure provided by the IVUS study with the spatial information presented in orthogonal angiographies. To achieve this integration, we first apply an image-based gating method, as proposed in [Maso Talou et al. 2014], to avoid artifacts in the reconstruction and also obtain a time coherent arrangement of the data. Then, we extract the vessel wall from the IVUS study over the intrinsic coordinates system defined along the transducer trajectory. Later we reconstruct this trajectory in a global coordinates system using orthogonal angiographies, where, finally, the IVUS segmentation is mapped to.

The paper is organized as follows. In Section 2, the three steps of the proposed reconstruction methodology are presented. In Section 3, preliminary results of the gating and reconstruction strategies are shown, and a discussion of these preliminary results is conducted.

2. Proposed methodology

2.1. Image-based gating for IVUS study

Generation of the motion signal Similarly to other image-based approaches, we construct a motion signal to identify the steadiest frame (frame with minimum displacement of structures accordingly to its adjacent frames) in each cardiac cycle, which is associated with the end-diastolic phase. For this, let us define the *motion signal* as a function $s(n)$ that measures the motion of the n-th image of the IVUS study. The signal $s(n)$ is chosen to be the linear combination of M image features, $s_i(n)$, $i = 1, \ldots, M$, characterizing the motion in an image, with coefficients $w_i \in (0, 1)$, as the weight factor of the feature s_i.

In this work two features are proposed. The first feature, $\hat{s}_0(n)$, is the 2D cross-correlation presented in [Winter et al. 2003]. The choice of this feature is reasonable because absence of movement is associated with two almost identical images, and as the motion increases between the images, the matching of structures decreases leading to a

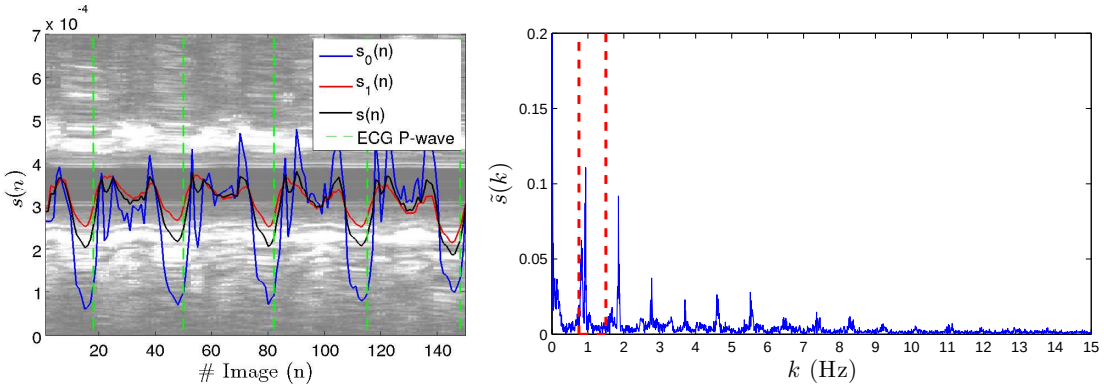

Figure 1. (Left) Longitudinal view of an IVUS study presenting the motion signal $s(n)$ and the associated features, $s_0(n)$ and $s_1(n)$, using $\alpha = 0.25$. Also the P-wave occurrence from the synchronized ECG is marked. (Right) Motion signal in the frequency domain where the red lines depict the range of physiologically valid heart frequencies.

smaller correlation. The second feature, $\hat{s}_1(n)$, measures the blurring in the image,

$$\hat{s}_1(n) = -\sum_{i=1}^{H}\sum_{j=1}^{W} |\nabla u_n(i,j)| \ , \tag{1}$$

which explores the fact that the movement of the transducer provokes a smoothing at the borders of the structures. To combine these features, we normalize them as

$$s_i(n) = \frac{\hat{s}_i(n) - \min_{1\leq n\leq N}(\hat{s}_i(n))}{\sum_{n=1}^{N}\hat{s}_i(n)} \tag{2}$$

where N is the number of images in the IVUS study. This last step ensures that all s_i are of the same order of magnitude. For the particular case of using two image features, the weight factors can be reduced to only one parameter, α, defined as $w_0 = \alpha$ and $w_1 = 1 - \alpha$.

The proposed signals are presented in Fig. 1 for an in-vivo study. It is observed that several consecutive columns, preceding certain points of minima, present a similar intensity pattern, meaning that the transducer is acquiring an almost invariant set of structures. In the signal $s(n)$, as well as in the individual features, a pseudo-periodical pattern of minima coincident with the end-diastolic phase (P-wave mark in Fig. 1) is observed.

End-diastolic phase identification The motion signal generated contains many undesirable local minima in each heartbeat, making the automatic selection a non-trivial task. Taking advantage of the pseudo-periodicity in $s(n)$, the frequency spectrum of the signal $\tilde{s}(k)$ is used to reconstruct a low frequency version of $s(n)$ eliminating spurious minima.

The frequency spectrum of the signal $\tilde{s}(k)$ is computed as the discrete Fourier transform of $s(n)$. As shown in Fig. 1, the spectrum presents a maximum frequency f_m in the range of physiologically valid heartbeat frequencies, i. e., $[0.75$ Hz - 1.66 Hz$]$. This frequency is a close approximation of the mean heart frequency along the entire study. For this, we introduce a factor, $\delta\, f_m,\ \delta \in (0,1)$, which models the deviation of the heartbeat

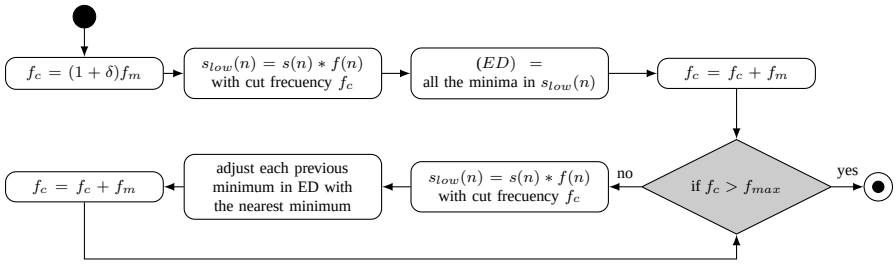

Figure 2. Activity diagram detailing the iterative adjustment of the minima from the initial signal $s_{low}(n)$ to $s(n)$. The variable ED represents the set of minima associated with the end-diastolic phase.

frequency along the study. Thus, we define the cut frequency for the low-pass filter as $f_c = (1+\delta)f_m$.

Then, the low frequency signal, $s_{low}(n)$, is constructed as the convolution $s_{low}(n) = s(n) * f(n)$, using the low-pass kernel $f(n)$ defined as

$$f(n) = \left[0,54 - 0,46\cos\left(2\pi\frac{n}{N}\right)\right]\left[\frac{f_c}{f_{max}}\text{sinc}\left(\frac{f_c n}{f_{max}}\right)\right]. \tag{3}$$

where f_{max} is the maximum frequency in the study calculated as half of the transducer frame rate and N is the number of images in the IVUS study.

The obtained $s_{low}(n)$ signal presents only one minimum for each heartbeat, allowing an initial approximation for the minima locations. As seen in Fig. 3, this approximation can be displaced from the pseudo-periodical minima of $s(n)$ due to the absence of high frequency contributions. For this reason, the iterative procedure presented in Fig. 2 is applied. At each step, the frequencies up to the next harmonic component are incorporated into the definition of $s_{low}(n)$ and each minimum location is adjusted to the nearest local minimum. This process is repeated until $s_{low}(n)$ incorporates all the harmonic components of f_m obtaining the adjusted minima in each heartbeat (see Fig. 3).

Decomposition in cardiac phases The identification of the images corresponding to the end-diastolic phase, allows the construction of sets of images associated to each heartbeat. Over these new sets of images, we define $\text{HB}(j,n)$ as the index (or number of frame) in the original IVUS study of the n-th image corresponding to the j-th heartbeat in the study, where $n = 1$ represents the images at the end-diastolic phase. Additionally, each set is decomposed in P cardiac phases of equal proportional duration, according to the indexation $m = 1,\ldots,B,\ k = 1,\ldots,P$

$$\text{CP}(k,m) = \text{HB}(m,1) + \text{round}\left(\frac{\text{HB}(m+1,1) - \text{HB}(m,1)}{P}(k-1)\right) \tag{4}$$

where $\text{CP}(k,m)$ is the index of the m-th image associated to the k-th cardiac phase and B is the quantity of heartbeats identified in the study. For this decomposition, an image could belong to more than one cardiac phase (if P is greater than the number of images in a heartbeat) but each cardiac phase is only associated with one image per heartbeat. This is to preserve an homogeneous axial spacing between the images in the same cardiac

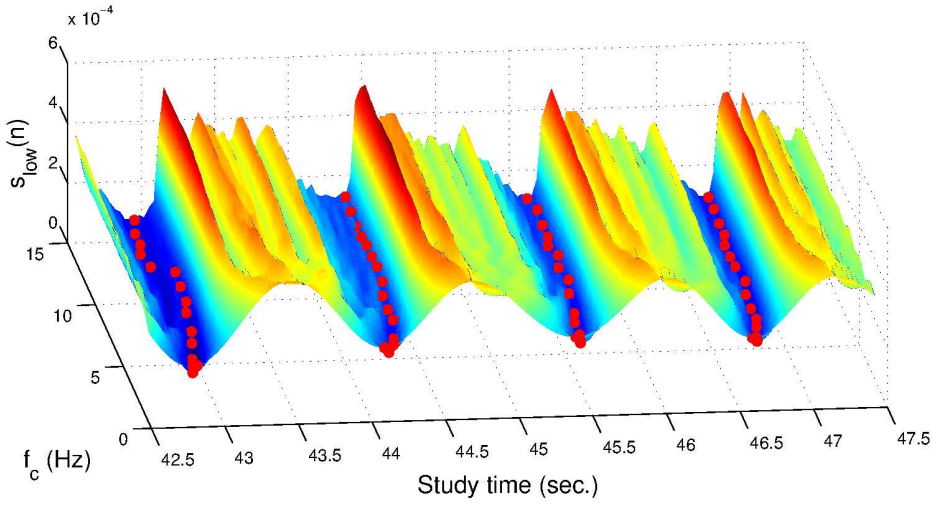

Figure 3. Evolution of the iterative adjustment scheme. The axis f_c corresponds to the cut frequency of the low-pass filter and, at each fixed value of this axis, the $s_{low}(n)$ associated signal is presented. The red dots mark the position of the adjusted minima corresponding to the end-diastolic phase.

phase. Finally, the set of images $U^k(m)$ corresponding to the k-th cardiac phase is defined as $U^k(m) = I(\mathrm{CP}(k, m))$, $m = 1, \cdots, B$.

2.2. Segmentation of IVUS gated studies

For the segmentation of the vessel wall, we use an active contour strategy proposed in [Maso Talou 2013] derived from [Kass et al. 1988, Xu and Prince 1998]. A suitable border map of the endothelial layer (EL) and the external elastic membrane (EEM) is obtained by an anisotropic oriented filter [Krissian et al. 2007], which is applied as a pre-processing step. Anisotropic oriented methods have shown an enhancement of the edges sharpness and a major homogenization of the tissue intensity pattern [Finn et al. 2011, Michailovich and Tannenbaum 2006]. Furthermore, by proper tailoring of the active contour functional, we avoid the collapse between the segmented contours of the EL and EEM.

The user interaction with this task is dramatically reduced by segmenting the frames sequentially and using the previous frame segmentation as initialization. This strategy is very effective due to the previous gating process where we remove the misalignment of the EL and EEM boundaries among adjacent frames. In this scenario, the user only has to indicate a few EL and EEM boundary points to initialize the active contour segmentation in the first frame and other frames where the segmentation has failed and a reinitialization is needed.

2.3. Registration of IVUS segmentation on angiography

As initial step, we determine the transducer path by segmenting the catheter deployed with the transducer in the distal position just before performing the IVUS acquisition. Particularly, we use a biplane snake as presented in [Cañero et al. 2000] which, in contrast with epipolar geometry approaches [Slager et al. 2000], allows to easily deal with orthogonal angiografies that are not acquired at the same time.

The mapping of the IVUS segmentation is performed by calculating the Frenet-Serret frame over the transducer path. With the orthogonal coordinate system determined by the tangent, normal and binormal vectors, we map the x and y Cartesian axes of the IVUS images to the normal and binormal axes at each point.

At last, we perform an optimization process to determine the correct rotation of the cross-sectional area segmented of the vessel around the transducer path, as presented in [Giannoglou et al. 2006]. To improve the robustness of the optimization process due to transducer/vessel displacement during the acquisition, an error based on the whole vessel projected area is used [Maso Talou 2013], instead of the error based on the projection of each contour projection in a fixed position.

3. Results and Discussion

The IVUS equipment used in this work is a station iLab Ultrasound Imaging System of Boston Scientific Corporation with a catheter Atlantis SR Pro with a transducer of 40 MHz. The acquisition was performed during a normal hemodynamic intervention procedure, acquiring orthogonal angiographies of the transducer location before the IVUS pullback.

In the image gating process, the IVUS study was decomposed into 33 cardiac phases. From these cardiac phases, we identified sets of images U^1 associated with the end-diastolic phase and U^{10} close to the ventricular systole. The longitudinal views of U^1 and U^{10} and the corresponding segmentations are presented in Figure 4. It can be noted a dramatical decrease of the transducer motion (visualized as oscillations of the EL and EEM structures) due to the time coherent decomposition performed by the gating method over the original IVUS study. Furthermore, this coherent decomposition facilitates with respect to the segmentation of the structure because of the alignment achieved and the low morphological variation from adjacent frames.

After applying the mapping process presented in Section 2.3, the 3D reconstruction of the coronary vessel is obtained (see Figure 5) allowing a correct deployment of the vessel wall structures in three-dimensional space. By repeating this registration process for all U^k subsets, a reconstruction of the vessel wall along the whole cardiac cycle is obtained.

4. Conclusions

The proposed methodology is capable to obtain patient specific vessel geometries coherently placed in space and in time. This has been achieved through the integration of IVUS and angiographic studies. The results obtained indicate that it is possible to facilitate percutaneous interventions for complex scenarios by visualizing the vessel not only in the space but also in time along the cardiac cycle (as long as the segmentation and registration is performed for each cardiac phase).

The relevance goes beyond the mere visualization of the vessel. The spatial deployment of the vessel improves the accuracy of volumetric measurements used for assessment of morphologic and morphometric quantities (for example, atherosclerotic plaque quantification and lesion extension). From this measurements, indexes for assessment of the plaque vulnerability are constructed, which are key for treatment evaluation.

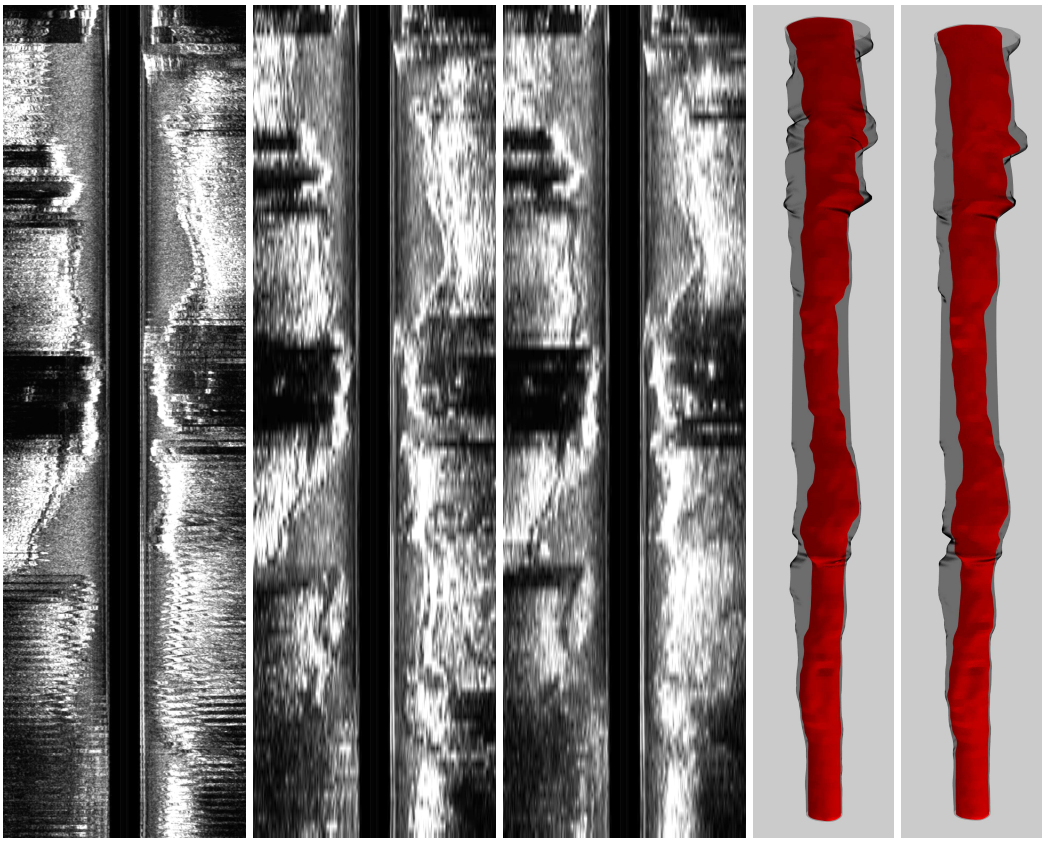

Figure 4. From left to right: longitudinal view of in-vivo IVUS study; longitudinal view of cardiac phase subset U^1; longitudinal view of cardiac phase subset U^{10}; segmentation of cardiac phase subset U^1; segmentation of cardiac phase subset U^{10}. In the segmentations, the translucent and red surfaces represent the EEM and the EL, respectively.

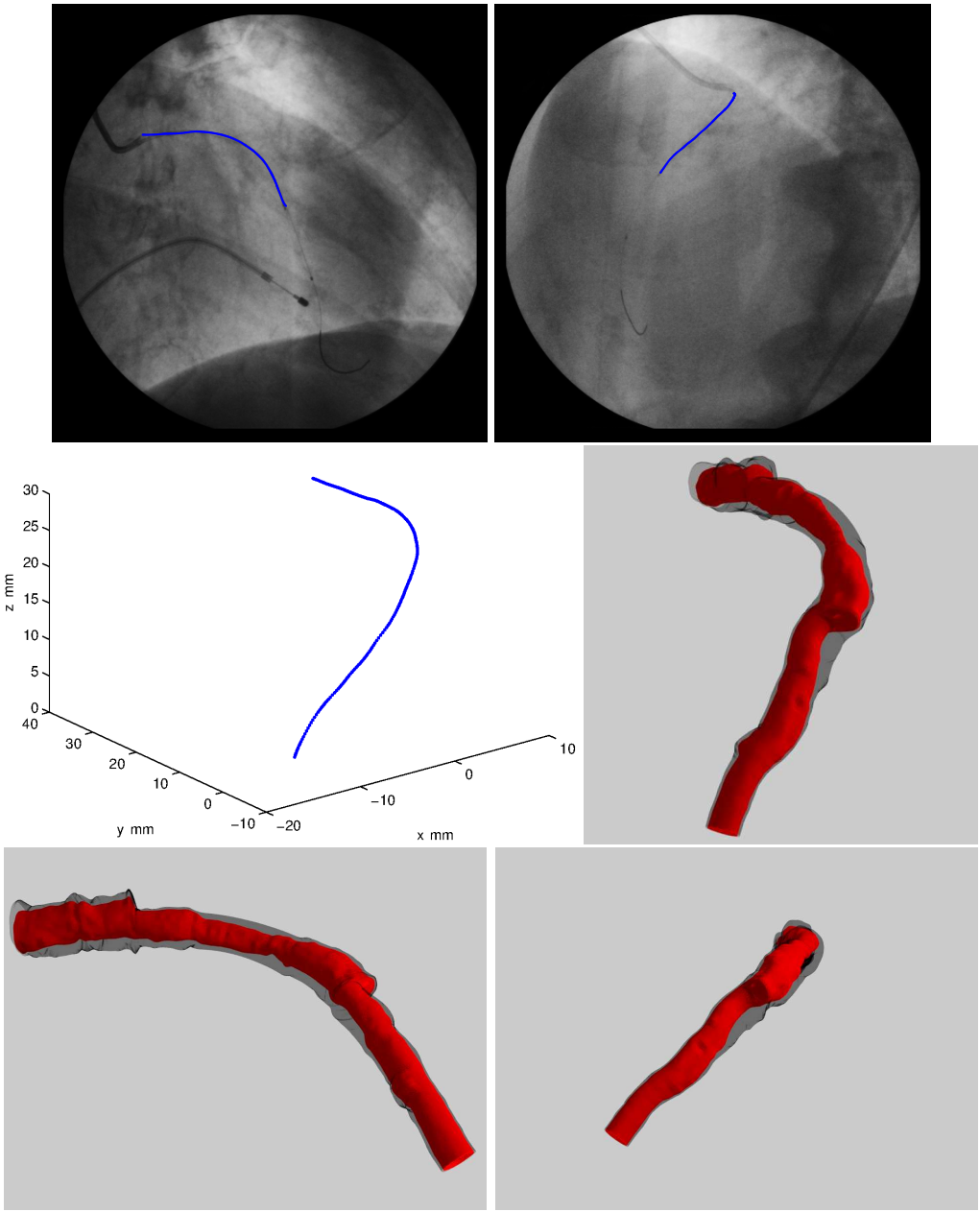

Figure 5. (Top) Orthogonal angiographies presenting the projection of 3D catheter segmentation (blue line); (center-left) 3D visualization of the resulting catheter segmentation; (center-right) final reconstruction of the vessel due to the mapping of the IVUS segmentation over the catheter segmentation; (bottom) final reconstruction of the vessel visualizing from the orthogonal angiographic angles.

As well, it also permits error comparison in the identification of vessel wall structures against other imaging techniques, less invasive but less accurate as well, such as magnetic resonance imaging or x-ray computed tomography.

Finally, the detailed vessel geometry obtained provides a high accurate input to conduct computational hemodynamic simulations in patient specific scenarios, being this of paramount importance for a mechanical evaluation of plaque evolution and vulnerability research, as we initially motivate.

5. Acknowledgements

This research was partially supported by the Brazilian agencies CNPq, FAPERJ and CAPES. The support of these agencies is gratefully acknowledged.

References

Cañero, C., Radeva, P., Toledo, R., Villanueva, J. J., and Mauri, J. (2000). 3d curve reconstruction by biplane snakes. *In Proc. IEEE of ICPR*, pages 563–566.

Carlier, S. G., van Damme, L. C. a., Blommerde, C. P., Wentzel, J. J., van Langehove, G., Verheye, S., Kockx, M. M., Knaapen, M. W. M., Cheng, C., Gijsen, F., Duncker, D. J., Stergiopulos, N., Slager, C. J., Serruys, P. W., and Krams, R. (2003). Augmentation of wall shear stress inhibits neointimal hyperplasia after stent implantation: inhibition through reduction of inflammation? *Circulation*, 107(21):2741–6.

Caro, C. G. (2009). Discovery of the role of wall shear in atherosclerosis. *Arterioscler., Thromb., Vasc. Biol.*, 29(2):158–61.

Chatzizisis, Y. S., Jonas, M., Coskun, A. U., Beigel, R., Stone, B. V., Maynard, C., Gerrity, R. G., Daley, W., Rogers, C., Edelman, E. R., Feldman, C. L., and Stone, P. H. (2008). Prediction of the localization of high-risk coronary atherosclerotic plaques on the basis of low endothelial shear stress: an intravascular ultrasound and histopathology natural history study. *Circulation*, 117(8):993–1002.

Feldman, C. L., Ilegbusi, O. J., Hu, Z., Nesto, R., Waxman, S., and Stone, P. H. (2002). Determination of in vivo velocity and endothelial shear stress patterns with phasic flow in human coronary arteries: A methodology to predict progression of coronary atherosclerosis. *Am Heart J*, 143(6):931–939.

Finn, S., Glavin, M., and Jones, E. (2011). Echocardiographic speckle reduction comparison. *Ultrasonics, Ferroelectrics and Frequency Control, IEEE Transactions on*, 58(1):82 –101.

Giannoglou, G. D., Chatzizisis, Y. S., Sianos, G., Tsikaderis, D., Matakos, A., Koutkias, V., Diamantopoulos, P., Maglaveras, N., Parcharidis, G. E., and Louridas, G. E. (2006). In-vivo validation of spatially correct three-dimensional reconstruction of human coronary arteries by integrating intravascular ultrasound and biplane angiography. *Coronary Artery Dis*, 17(6):533–543.

Honda, Y. and Fitzgerald, P. J. (2008). Frontiers in intravascular imaging technologies. *Circulation*, 117(15):2024–37.

Kass, M., Witkin, A., and Terzopoulos, D. (1988). Snakes: active contour models. *Int J Comput Vision*, pages 321–331.

Krissian, K., Westin, C., Kikinis, R., and Vosburgh, K. (2007). Oriented speckle reducing anisotropic diffusion. *IEEE Trans. Image Processing*, 16(5):1412–1424.

Maso Talou, G. D. (2013). Ivus images segmentation driven by active contours and spacio-temporal reconstruction of the coronary vessels aided by angiographies. Master's thesis (in portuguese), National Laboratory for Scientific Computing.

Maso Talou, G. D., Larrabide, I., Lemos, P. A., Blanco, P. J., and Feijóo, R. A. (2014). Decomposition of ivus studies in cardiac phases. In *Proceedings of the 1st Biomedical Signal Analysis Conference (Florianópolis, March 25-28)*.

Michailovich, O. and Tannenbaum, A. (2006). Despeckling of medical ultrasound images. *IEEE Trans. Ultrason Ferroelectrics Freq Contr*, 53(1):64 –78.

Naghavi, M., Libby, P., Falk, E., et al. (2003). From vulnerable plaque to vulnerable patient: a call for new definitions and risk assessment strategies. *Circulation*, 108(15):1772–8.

Slager, C. J., Wentzel, J. J., Schuurbiers, J. C. H., Oomen, J. A. F., Kloet, J., Krams, R., von Birgelen, C., van der Giessen, W. J., Serruys, P. W., and de Feyter, P. J. (2000). True 3-dimensional reconstruction of coronary arteries in patients by fusion of angiography and ivus (angus) and its quantitative validation. *Circulation*, 102:511–516.

Stone, P. H., Coskun, A. U., Kinlay, S., Clark, M. E., Sonka, M., Wahle, A., Ilegbusi, O. J., Yeghiazarians, Y., Popma, J. J., Orav, J., Kuntz, R. E., and Feldman, C. L. (2003). Effect of endothelial shear stress on the progression of coronary artery disease, vascular remodeling, and in-stent restenosis in humans: in vivo 6-month follow-up study. *Circulation*, 108(4):438–44.

Wentzel, J. J., Janssen, E., Vos, J., Schuurbiers, J. C. H., Krams, R., Serruys, P. W., de Feyter, P. J., and Slager, C. J. (2003). Extension of increased atherosclerotic wall thickness into high shear stress regions is associated with loss of compensatory remodeling. *Circulation*, 108(1):17–23.

Wentzel, J. J., Kloet, J., Andhyiswara, I., Oomen, J. a. F., Schuurbiers, J. C. H., de Smet, B. J. G. L., Post, M. J., de Kleijn, D., Pasterkamp, G., Borst, C., Slager, C. J., and Krams, R. (2001). Shear-Stress and Wall-Stress Regulation of Vascular Remodeling After Balloon Angioplasty : Effect of Matrix Metalloproteinase Inhibition. *Circulation*, 104(1):91–96.

Winter, S. A. D., Hamers, R., Degertekin, M., Tanabe, K., Lemos, P. A., Serruys, P. W., and Roelandt, J. (2003). A Novel Retrospective Gating Method for Intracoronary Ultrasound Images based on Image Properties. pages 13–16.

Xu, C. and Prince, J. L. (1998). Snakes, shapes, and gradient vector flow. *IEEE Trans. on Image Processing*, 7(3):359–369.